Low x Physics at HERA

Joanne Cole

University of Bristol
H. H. Wills Laboratory, Tyndall Avenue, Bristol, BS8 1TL, UK

Abstract

Recent measurements made in the low x region at HERA are presented. The latest structure function results are reviewed and then used as the basis for a study of the transition region at very low Q^2. QCD dynamics beyond the DGLAP formalism are then discussed, with emphasis on the search for evidence of saturation effects and BFKL dynamics.

1 Introduction

Deep inelastic lepton-nucleon scattering provides the perfect environment in which to investigate the internal structure of hadrons including the applicability of the theory which governs their interactions, Quantum Chromodynamics (QCD). While the fixed-target deep inelastic scattering (DIS) experiments provided a wealth of information, including the observation of Bjorken scaling [1], the kinematic region in which investigations could be made was limited to higher x values. The advent of the HERA ep collider has substantially extended the kinematic region of study, opening up the low x regime for the first time.

Since the first observation of the strong rise of the structure function F_2 at low x by the H1 and ZEUS Collaborations [2], much progress has been made in the understanding of the low x region and many high precision measurements are available. The evolution of F_2 is well described by the perturbative QCD DGLAP equations [3] over a wide range in the photon virtuality, Q^2, including down to values as small as 1.5 GeV. However, at the lowest values of Q^2 deviations from the DGLAP predictions are observed, indicating a transition from the perturbative to the non-perturbative regime. In the latter only phenomenological models, such as those inspired by Regge theory [4], are available to describe the data.

Although the DGLAP evolution equations have been remarkably successful in fitting the HERA data, they only resum terms in $\ln Q^2$ and ignore terms in $\ln 1/x$. In the low x regime, the terms in $\ln 1/x$ are expected to become important [5] and therefore evolution equations which account for these terms should also be tested. It is also possible that gluon recombination effects (so-called "saturation" effects) should be visible in the low x regime [6, 7, 8].

This paper presents a wide range of HERA results, including the high precision measurements of the structure function F_2 and its local derivatives and the data from the transition region between perturbative and non-peturbative QCD. One possible test of alternative QCD evolution equations is discussed.

2 Kinematics and Cross Sections

Deep inelastic scattering (DIS) of positrons on protons is shown in figure 1. Such interactions are generally considered in terms of any two of the following three invariant kinematic variables: Q^2, the virtuality of the exchanged photon; x, the Bjorken scaling variable and y, the inelasticity variable.

These variables are related by $Q^2 = xys$ where s is the ep centre-of-mass energy. Another useful variable is $W^2 = (q+p)^2$, which is the square of the $\gamma^* p$ centre-of-mass energy.

The double differential neutral current ep cross section at low Q^2 may be written as

$$\frac{d^2\sigma^{e^+p}}{dxdQ^2} = \frac{2\pi\alpha^2}{xQ^4}[Y_+ F_2 - y^2 F_L] \tag{1}$$

where $Y_\pm = 1 \pm (1-y)^2$ and F_L is the longitudinal structure function. The contribution from Z^0 exchange has been neglected.

In the naive Quark-Parton model, $F_2(x) = x\sum_i e_i^2 q_i(x)$, where $q_i(x)$ refer to the parton distributions of type i and e_i are the corresponding quark charges. In the same model the Callan-Gross relation [9] holds meaning that $F_L = 0$. In the QCD-improved parton model, F_L can be large. However, because of the y^2 multiplier the contribution of F_L to the cross section at low y is small.

Some results use an alternative form of the double differential cross section, the so-called reduced cross section, which is defined as

$$\sigma_r \equiv \frac{Q^4 x}{2\pi\alpha^2 Y_+}\frac{d^2\sigma}{dxdQ^2} = F_2 - \frac{y^2}{Y_+}F_L \tag{2}$$

The double differential cross section can also be written as

$$\frac{d^2\sigma^{e^+p}}{dxdQ^2} = \Gamma[\sigma_T^{\gamma^*p}(W^2,Q^2) + \varepsilon\sigma_L^{\gamma^*p}(W^2,Q^2)] \tag{3}$$

where $\Gamma = \alpha Y_+/2\pi Q^2 y$ and $\varepsilon = 2(1-y)/Y_+$. $\sigma_T^{\gamma^*p}$ and $\sigma_L^{\gamma^*p}$ are the transverse and longitudinal contributions to the total γ^*p cross section respectively. At low Q^2, $\sigma_{TOT}^{\gamma^*p} = \sigma_T^{\gamma^*p} + \sigma_L^{\gamma^*p} \approx \frac{4\pi^2\alpha}{Q^2}F_2$.

3 Theoretical Background

The DIS cross section can be expressed as a convolution of the partonic cross section, which can be calculated in perturbative QCD, and the parton densities, f, which are non-perturbative. When the photon is highly virtual it is assumed that the parton densities satisfy the DGLAP equations, which are represented by the schematic equation

$$\frac{df}{d\ln Q^2} \sim f \otimes \mathcal{P} \tag{4}$$

where $\mathcal{P}$ is a splitting function or the probability that a given parton will split into two others and $\otimes$ indicates the convolution of the two quantites.

At sufficiently low x, the $\ln 1/x$ terms will become more important than the $\ln Q^2$ terms in the perturbative expansion. In this region the BFKL evolution scheme [5], which resums the $\ln 1/x$ terms, rather than the $\ln Q^2$ terms, should be applicable. It is therefore expected that this scheme should take over from DGLAP evolution at very low x.

In the low Q^2 region only non-perturbative models can be used, such as those inspired by Regge theory. These models are based on the exchange of a "colourless" object, generically referred to as the Pomeron. These models are applicable in the region where $s >> Q^2$ or $x << 1$, ie. exactly the region of interest in this paper. Such models predict the energy dependence of the total cross section to be

$$\sigma_{TOT}^{\gamma^* p} \sim A(W^2)^{\alpha_{I\!R}(0)-1} + B(W^2)^{\alpha_{I\!P}(0)-1} \tag{5}$$

where $\alpha_{I\!P}(0) > 1$ and $\alpha_{I\!R}(0) < 1$ are the Pomeron and Reggeon intercepts respectively.

Another approach can also be considered in the low Q^2 region, which is known as the Colour Dipole picture (CDP). Here, the *ep* interaction is viewed in the proton rest frame, rather than the infinite momentum frame. In this type of model, the virtual photon fluctuates into a quark-antiquark dipole a long way upstream of the proton. This dipole then interacts with the proton. The cross section is driven by the dipole cross section $\sigma_{dipole}(x, r)$ where r is the dipole radius, which is inversely proportional to Q.

At small r (the perturbative QCD region) the dipole cross section varies as r^2, while at large r the dipole cross section becomes constant or saturates. This model is applicable at both low and high Q^2.

4 HERA Data

Prior to 1998 HERA collided 27.5 GeV positrons with 820 GeV protons. After that the proton beam energy was increased to 920 GeV. During 1998 and part of 1999 an electron beam was used. During the rest of 1999 and the whole of the 2000 data-taking period HERA returned to using a positron beam. The majority of the results discussed in this paper are based on the 1996-97 data, although some results use the data taken in later periods. The pre-1998 data corresponds to 40-50 pb^{-1} per experiment, while the post-1998 electron data corresponds to approximately 16 pb^{-1} per experiment. The post-1998 positron data corresponds to approximately 67 pb^{-1} per experiment.

The results presented in the subsequent sections are based on several different subsets of the data samples just described. These subsets are selected according to the following criteria:

BPC/BPT: This label indicates data taken by the ZEUS Collaboration in which the outgoing positron is scattered through very small angles. In such events, the scattered positron is detected in the BeamPipe Calorimeter [10], which is situated just outside the main calorimeter. Small scattering angles correspond to low Q^2: the data in this subset lie in the range $0.045 < Q^2 < 0.65$ GeV^2;

ISR: This label indicates data taken by the H1 Collaboration in which a hard initial state photon is radiated. ISR photons are emitted collinear to the incoming positron beam and therefore escape down the beampipe. They are detected in the luminosity monitor, which is situated downstream of the main detector. The emission of the photon effectively lowers the centre-of-mass energy of the interaction and therefore results in data which extend to lower Q^2 values than non-radiative events. The data in this subset lie in the range $0.35 < Q^2 < 20$ GeV^2;

SVTX: This label indicates data taken by both Collaborations in which the interaction vertex was shifted by 70 cm from its nominal position. If the vertex is shifted in the outgoing proton direction, the acceptance of the detector is increased to accomodate small positron scattering angles and hence lower Q^2 values are accessible. The data in this subset lie in the range $0.6 < Q^2 < 17$ GeV^2 (ZEUS) or $0.5 < Q^2 < 3.5$ GeV^2 (H1);

Nominal: This indicates standard DIS data in which no special measures have been taken to extend the Q^2 range. For the H1 Collaboration this means data with $Q^2 = 1.5$ GeV^2 and upwards. For the ZEUS Collaboration the lowest value used is $Q^2 = 2.7$ GeV^2.

5 F_2 Measurements

Figure 2 shows HERA measurements of $F_2(x, Q^2)$ as a function of x at $Q^2 = 15$ GeV^2. The results from the two Collaborations are in excellent agreement and there is also a small overlap with the fixed target data [11, 12, 13] which are also shown in the figure. The HERA data have a typical precision of 3 %.

The strong rise with decreasing x shown in figure 2 can be parametrised as $x^{-\lambda}$. This shape is well described by two different next-to-leading order (NLO) DGLAP predictions [15, 16].

A wider range of $F_2(x, Q^2)$ measurements are presented in figure 3, which shows the dependence of $F_2(x, Q^2)$ on Q^2. A large number of HERA measurements are shown, along with data from the fixed target experiments BCDMS [11], E665 [12], SLAC [14] and NMC [13].

The results are compared to three different theoretical predictions. The first (labelled "H1 QCD") is the result of a NLO DGLAP fit made by the H1 Collaboration [17]. The second prediction (labelled "CSST") is based on the Colour Dipole model of Cvetic et al. [7]. The third prediction (labelled "ZEUS Regge97") is the result of a fit to ZEUS BPC data, which is based on Regge Theory [18]. This fit assumes that the γp cross section is given by equation 5 and that it is related to the total $\gamma^* p$ cross section by

$$\sigma_{TOT}^{\gamma^* p} = \frac{M_0^2}{M_0^2 + Q^2} \cdot \sigma_0^{\gamma p}(W^2) \tag{6}$$

where M_0^2 and $\alpha_{I\!P}(0)$ are free parameters of the fit. The fit yields $M_0^2 = 0.52 \pm 0.04$ GeV^2 and $\alpha_{I\!P}(0) = 1.102 \pm 0.007$.

The results are well-described by all three models in the regions in which they are applicable. The predictions cover a wide range in both x and Q^2. The previously reported scaling violations are also visible. It is evident that the slope of the data is flatter at low Q^2 than at high Q^2.

6 The Extraction of F_L

In order to measure F_L at HERA, data with a range of y values for a given x and Q^2 are required. This requires datasets with different centre-of-mass energies. This can be achieved by using only events in which an ISR photon has been detected, as described in section 4. This, however, is a technically challenging analysis.

The H1 Collaboration have made an extraction of F_L, rather than a direct measurement, using their nominal dataset. There are two possible extraction methods, both of which use the reduced cross section, σ_r. Figure 4 demonstrates the first of these two methods. It shows σ_r as a function of x for $Q^2 = 20$ GeV^2. The data are compared to the H1 NLO DGLAP fit, described earlier. A turnover is visible at low x (high y). A second fit is also shown in which $F_L = 0$. This fit overshoots the data at low x. The difference is caused by the F_L contribution to σ_r and therefore F_L can be extracted using:

$$F_L = \frac{Y_+}{y^2} \cdot (F_2^{QCDfit} - \frac{xQ^4}{2\pi\alpha^2}\sigma_r) \tag{7}$$

The second method uses the derivative of σ_r with respect to $\ln y$, which is given by

$$\frac{d\sigma_r}{d\ln y} = \frac{dF_2}{d\ln y} - F_L \cdot 2y^2 \cdot \frac{2-y}{Y_+^2} + \frac{dF_L}{d\ln y} \cdot \frac{y^2}{Y_+} \tag{8}$$

This derivative has a stronger y dependence and is therefore more sensitive to F_L. The behaviour of the derivative is shown in figure 5. At low y the derivative is flat as a function of y and therefore a linear fit is made in this region from which F_L can be extracted at high y, where the derivative is no longer linear. This method is used at low Q^2, while the previous method is only used at higher Q^2, as the errors arising from the extrapolation of the $F_L = 0$ fit at low Q^2 are large.

The results from these two methods are shown in figure 6. This is the first attempt to investigate F_L at HERA and good agreement is seen with the predictions from NLO DGLAP evolution. However, it is clear that a direct measurement of F_L is needed.

7 The Transition Region

The total $\gamma^* p$ cross section can be extracted from the F_2 data discussed in section 5 using the relation

$$\sigma_{TOT}^{\gamma^* p} = \frac{4\pi^2\alpha}{Q^2} F_2 \tag{9}$$

These results are plotted as a function of Q^2 for different values of W in figure 7. This figure shows clearly the change in the slope with increasing Q^2, which was discussed in section 5. In the figure, the total cross section is compared to the same three theoretical predictions to which F_2 is compared in figure 3. It is interesting to note that the colour dipole model (CSST) does a reasonable job of describing the whole range of Q^2 in the figure. Results such as these lead to the question: At what point does the transition from non-perturbative to perturbative QCD take place ?

One way of answering this question is to look at the local derivatives of F_2. In this case, the derivative $\partial \ln F_2/\partial \ln x$ is the most useful. This derivative is equal to $-\lambda$, if it is assumed that $F_2 \sim x^{-\lambda}$, as predicted by perturbative QCD.

This derivative has been measured by both Collaborations; figure 8 shows the results from the H1 Collaboration. At higher Q^2 and low x, λ appears to be constant, as expected. The Q^2 dependence of λ can therefore be determined assuming $F_2(x, Q^2) = C(Q^2)x^{-\lambda(Q^2)}$. The results of a similar procedure, performed by the ZEUS Collaboration, are shown in figure 9.

The figure shows that at low Q^2, λ is independent of Q^2, as predicted by the Regge-inspired fit. At higher Q^2, the observed Q^2 dependence of λ is exactly that expected from perturbative QCD. The transition between the two occurs in the region around $Q^2 = 1$ GeV^2. Although the two different predictions describe the data well in their regions of applicability, there is no common model for describing both regimes and one is clearly needed. One potential contender could be the Colour Dipole model, one example of which (CSST) is already able to describe the results in figure 7.

Clearly, $\partial \ln F_2/\partial \ln x$ is not the only derivative which can be studied. The derivative, $\partial F_2/\partial \ln Q^2$, can provide information about the way the slope of F_2 changes with x, rather than Q^2.

It is clear that F_2 cannot continue to rise indefinitely and therefore it is expected that at low x "damping" or saturation effects should be visible. This would be observed in the behaviour of $\partial F_2/\partial \ln Q^2$ with x.

Figure 10 shows $\partial F_2/\partial \ln Q^2$ as a function of x at different values of Q^2 and compares them to the predictions of the NLO DGLAP fit made by the H1 Collaboration. The data are well described by the prediction, indicating that no damping effects are present down to $Q^2 \sim 3$ GeV^2.

The ZEUS Collaboration look at the same derivative in a different way, as shown in figure 11. Here, the derivative is plotted as a function first of Q^2, then of x for different values of W. In figure 11a it can be seen that at lower Q^2 (equivalent to low x in figure 11b) the derivatives tend to fall as Q^2 decreases and appear to become independent of W at $Q^2 \simeq 0.4$. Equally, figure 11b shows that at higher x, the derivatives tend to fall with increasing x and appear to become independent of x above $x \simeq 0.003$.

Leading order DGLAP evolution predicts at low x that [19]

$$\frac{\partial F_2}{\partial \log Q^2} \sim xg(x, Q^2) \tag{10}$$

which is consistent with the behaviour seen at higher x in figure 11b, providing the gluon density $xg(x, Q^2)$ has the form $x^{-\lambda}$ and only varies slowly with Q^2.

At low Q^2 a Colour Dipole picture (in this case the model of Golec-Biernat and Wüsthoff (GB&W [8]) is used) predicts that

$$\frac{\partial F_2}{\partial \log Q^2} \sim Q^2 \sigma_0 \tag{11}$$

where σ_0 indicates the total photoproduction cross section. This is an expression of electromagnetic current conservation and is consistent with the behaviour seen at low Q^2 in figure 11a, providing that σ_0 only has a weak x dependence.

In figure 11 the derivatives are compared to the GB&W model (dashed lines) and the NLO DGLAP-based fit from the ZEUS Collaboration [20]. Each model is shown only in the region in which it is applicable. The former predicts the same behaviour as DGLAP evolution in the region where the DGLAP equations are applicable, but also predicts the transition from that to the behaviour given in equation 11.

Both predictions give a reasonable description of the data. In fact, there is some indication of a turn-over also occurring in the DGLAP predictions, which is a result of the rapidly decreasing gluon density below $Q^2 = 10$ GeV^2. There is, therefore, no compelling evidence that one model describes the data better than the other. Further studies are needed before firm conclusions about the existence of saturation can be made.

8 Probing QCD Dynamics at low x

Although the majority of HERA low x results are well described by NLO DGLAP evolution, it is important to look for evidence of other evolution schemes. There are several evolution schemes available which apply in different kinematic regions, but only the BFKL scheme will be discussed here.

The onset of BFKL evolution should be most visible at very low x, as discussed earlier. BFKL evolution also predicts no strong ordering in the parton transverse momenta (k_T), therefore events in which $k_T \sim Q^2$ are the most likely in which to find the signature of BFKL dynamics. These requirements are best fulfilled by looking at jet production at low x and Q^2. In such events, transverse momentum can only be balanced if the jet is detected at small angles to the proton beam direction, the so-called "forward" region. The direction of the jet is defined in terms of its pseudorapidity, $\eta = -\ln\tan\theta/2$, where θ is the polar angle measured with respect to the proton beam direction. This means that jets detected in the forward region will have large, positive values of η.

The H1 Collaboration has performed an analysis of forward jet production, in which the jets are identified using the inclusive k_T algorithm [21]. Only events which satisfy $5 < Q^2 < 100$ GeV^2 and $0.2 < y < 0.6$ and which contain jets with $E_T > 5$ GeV are used. Jets in both the central and forward regions (defined by $0.5 < \eta_{jet} < 1.5$ and $1.5 < \eta_{jet} < 2.8$ respectively) were studied and the results compared to NLO DGLAP predictions [22].

One of the key issues in comparing these results to theory is the choice of renormalisation scale. Two different choices were considered: $\mu_R^2 = E_T^2$ and $\mu_R^2 = Q^2$. The differential jet cross sections with respect to the jet E_T are best described by NLO DGLAP when $\mu_R^2 = E_T^2$ [23]. When Q^2 is used there is a tendency for the theory to overshoot the data at high E_T, indicating that Q^2 may be too low to be the dominant scale in this region.

Figure 12 shows the comparison between data and theory as a function of Bjorken x. The inner, darker band represents the uncertainty arising from the hadronisation corrections which have been applied to the theory, while the lighter shaded area represents the total uncertainty, including that from μ_R. Figure 12 shows that when $\mu_R^2 = E_T^2$ is used (the preferred choice) the data is significantly higher than the predictions in the lowest x bins in the forward region. If $\mu_R^2 = Q^2$ is chosen, the uncertainty on the prediction is significantly larger and there is reasonable agreement with the data. If $\mu_R^2 = E_T^2$ is the correct choice of renormalisation scale, then the discrepancy at low x must be explained.

There are several possible explanations for the discrepancies observed in the $\mu_R^2 = E_T^2$ case. It may mean that higher order corrections are required, or that a resolved photon contribution is needed. It is not yet possible to verify if either of these explanations is correct. The results could, however, mean that BFKL dynamics are needed to properly describe the data.

9 Conclusions

Many aspects of low x physics and QCD have been studied at HERA, only a few of which have been presented here. Both the H1 and ZEUS Collaborations now have large datasets available, from which it has been possible to measure the structure function $F_2(x, Q^2)$ to high precision over a wide range in x and Q^2. This data is well-described by NLO DGLAP evolution at higher Q^2 and by Regge-inspired models at low Q^2. In both regions the data are well described by one version of the Colour Dipole picture.

The range over which data is now available has opened up the possibility to study the transition from non-perturbative to perturbative QCD, as well as to question whether physics beyond DGLAP evolution, such as BFKL dynamics or saturation, is needed or indeed observable at HERA. It is not possible to draw any conclusions yet, but the results presented here have certainly provided a tantalising glimpse of what may be possible using the data taken at HERA II.

References

[1] SLAC-MIT Collaboration, G. Miller et al.,Phys.Rev. **D5** (1972) 528

[2] H1 Collaboration, I. Abt et al., Nucl.Phys. **B407** (1993) 515; ZEUS Collaboration, M. Derrick et al.,Phys.Lett. **B316** (1993) 412

[3] L.N. Lipatov, Sov.J.Nucl.Phys. **20** (1975) 3; V.N. Gribov and L.N. Lipatov, Sov.J.Nucl.Phys. **15** (1972) 438; G. Altarelli and G. Parisi, Nucl.Phys. **B126** (1977) 298; Y.L. Dokshitzer, Sov.Phys. JETP **46** (1977) 641

[4] P.D.B. Collins, *An Introduction to Regge Theory and High Energy Scattering*, Cambridge University Press, 1977

[5] V.S. Fadin, E.A. Kuraev and L.N. Lipatov, Phys.Lett. **B60** (1975) 50; E.A. Kuraev, L.N. Lipatov and V.S. Fadin, Sov.Phys. JETP **44** (1976) 443; E.A. Kuraev, L.N. Lipatov and V.S. Fadin, Sov.Phys. JETP **45** (1977) 199; I.I. Balitsky and L.N. Lipatov, Sov.J.Nucl.Phys. **28** (1978) 822

[6] L.V. Gribov, E.M. Levin and M.G. Ryskin, Phys.Rep. **100** (1982) 1.

[7] D. Schildknecht, B. Surrow and M. Tentyukov, Mod.Phys.Lett. **A16** (2001) 1829; G. Cvetic, D. Schildknecht, B. Surrow and M. Tentyukov, Eur.Phys.J. **C20** (2001) 77; D. Schildknecht, B. Surrow and M.Tentyukov, Phys.Lett. **B499** (2001) 16

[8] K. Golec-Biernat and M. Wüsthoff, Phys.Rev. **D59** (1999) 014017; K. Golec-Biernat and M. Wüsthoff, Phys.Rev. **D60** (1999) 114023.

[9] C.G. Callan and D. Gross, Phys.Rev.Lett. **22** (1969) 156

[10] ZEUS Collaboration, J. Breitweg et al., Phys.Lett. **B407** (1997) 432

[11] BCDMS Collaboration, A.C. Benvenuti et al., Phys.Lett. **B223** (1989) 485; BCDMS Collaboration, A.C. Benvenuti et al., Phys.Lett. **B237** (1990) 592

[12] E665 Collaboration, M.R. Adams et al.,Phys.Rev. **D54** (1996) 3006

[13] NMC Collaboration, M. Arneodo et al., Nucl.Phys. **B483** (1997) 3

[14] L.W. Whitlow et al., Phys.Lett. **B282** (1992) 475

[15] A.D. Martin et al., Eur.Phys.J. **C14** (2000) 133

[16] H.L. Lai et al., Eur.Phys.J. **C12** (2000) 375

[17] H1 Collaboration, C. Adloff et al., Eur.Phys.J. **C13** (2000) 609

[18] ZEUS Collaboration, J. Breitweg et al., Phys.Lett. **B487** (2000) 53

[19] K. Prytz, Phys.Lett. **B311** (1993) 286

[20] ZEUS Collaboration, S. Chekanov et al., *The ZEUS NLOQCD fit to determine parton distribution functions and* α_s, abstract 628, proceedings of Int. Europhysics Conf. on High Energy Physics, Hungary 2001.

[21] S.D. Ellis and D.E. Soper, Phys.Rev. **D48** (1993) 3160; S. Catani, Y.L. Dokshitzer, M.H. Seymour and B.R. Webber, Nucl.Phys. **B406** (1993) 187

[22] S. Catani and M.H. Seymour, Nucl.Phys. **B485** (1997) 291; Erratum-ibid. **B510** (1997) 503

[23] H1 Collaboration, C. Adloff et al., *A Measurement of Single-Inclusive Jet Cross Sections in the Central and Forward Regions at low* x *in DIS at HERA*, abstract 999, proceedings of Int. Conf. on High Energy Physics, Japan, 2000

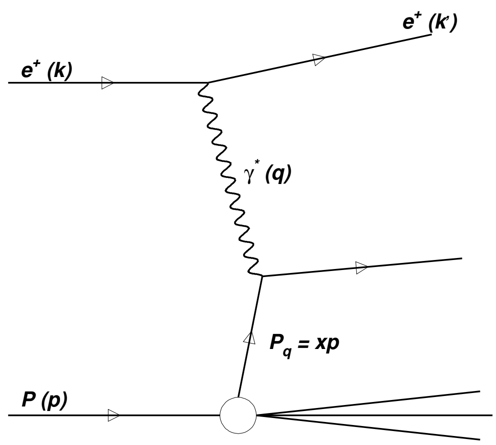

Figure 1: The deep inelastic interaction of a positron with four-momentum k with a proton of four-momentum p.

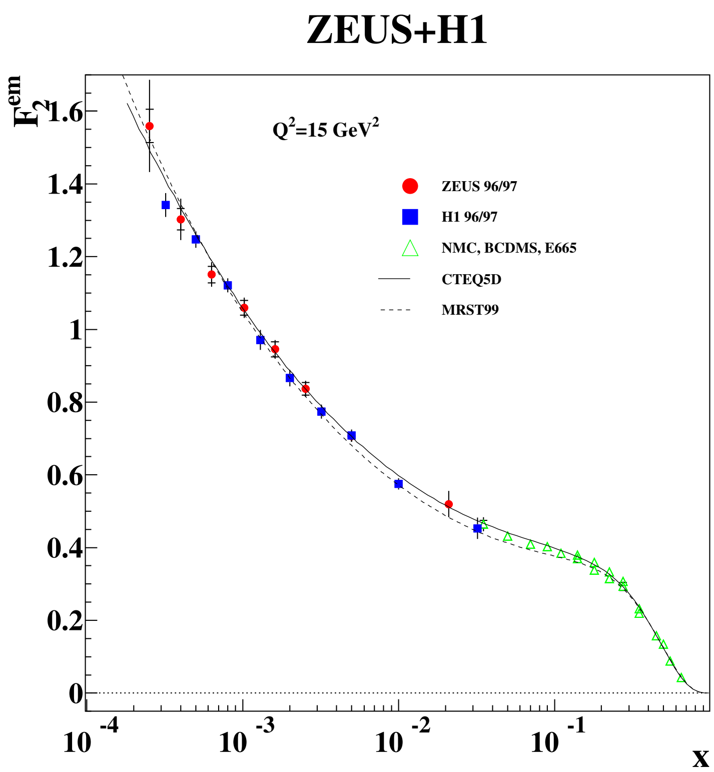

Figure 2: A summary of $F_2(x, Q^2)$ data at $Q^2 = 15$ GeV^2 as a function of x. The measurements are compared to two different DGLAP fits: one from the CTEQ group and one from MRST (see text).

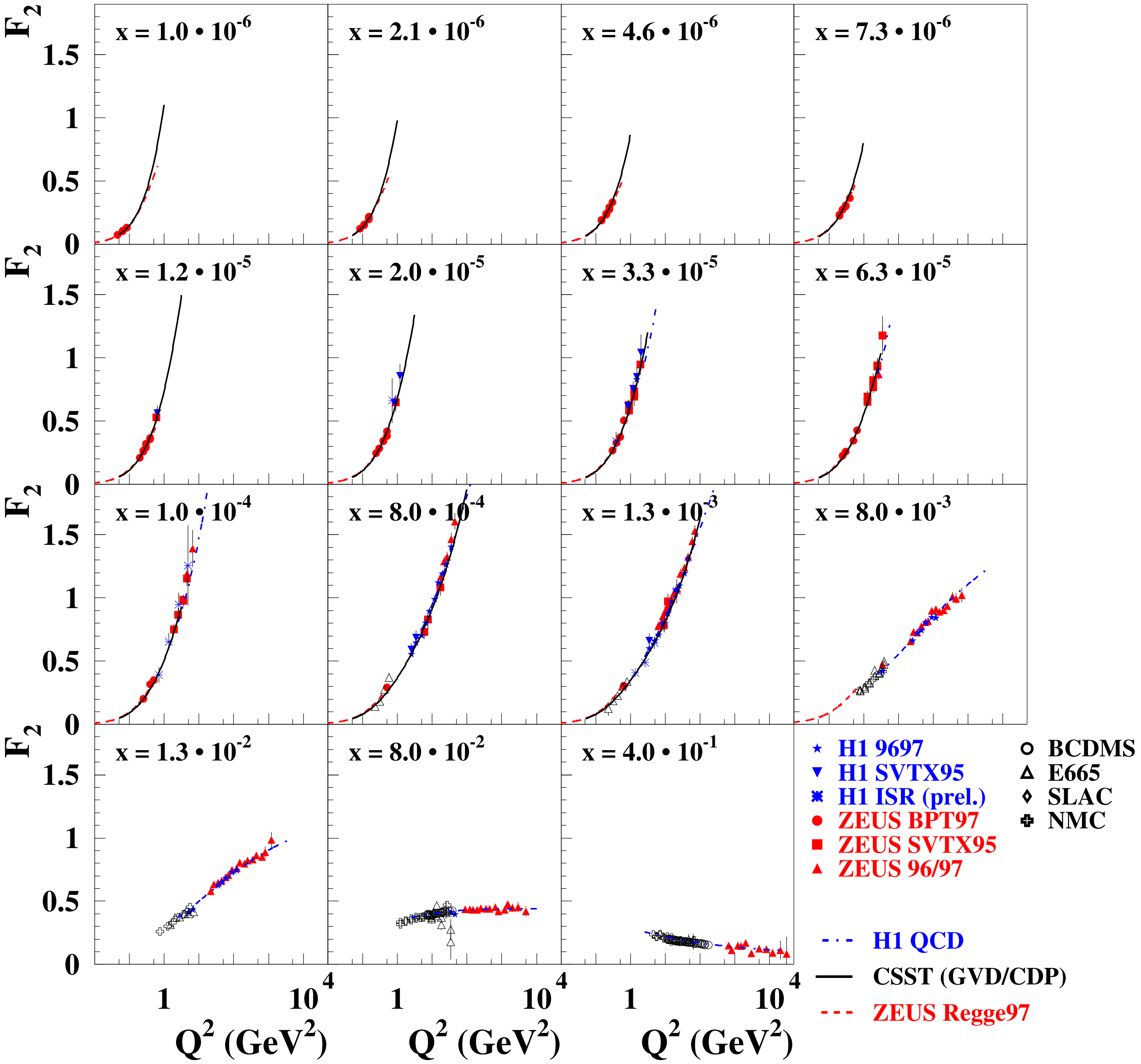

Figure 3: $F_2(x, Q^2)$ as a function of Q^2 for different values of x. Data from both HERA and fixed target experiments are shown. The measurements are compared to three different theoretical predictions, details of which are given in the text.

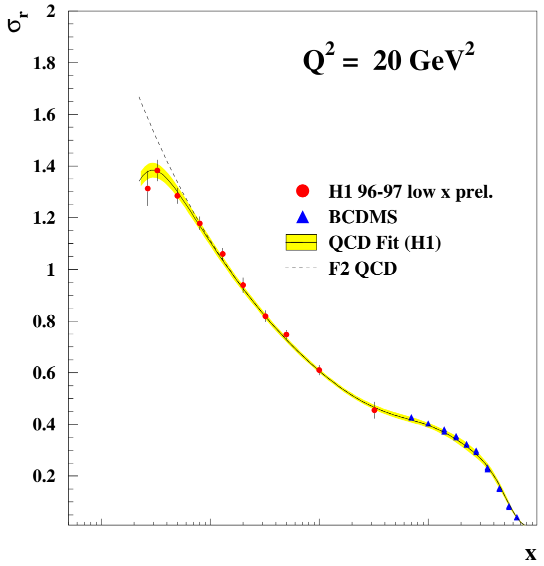

Figure 4: The reduced cross section, σ_r, from the H1 and BCDMS Collaborations, as a function of x at $Q^2 = 20$ GeV^2. The data are compared to a full QCD fit (solid band) and to a fit in which $F_L(x, Q^2) = 0$. The effect of $F_L(x, Q^2)$ is clearly visible at low x (high y).

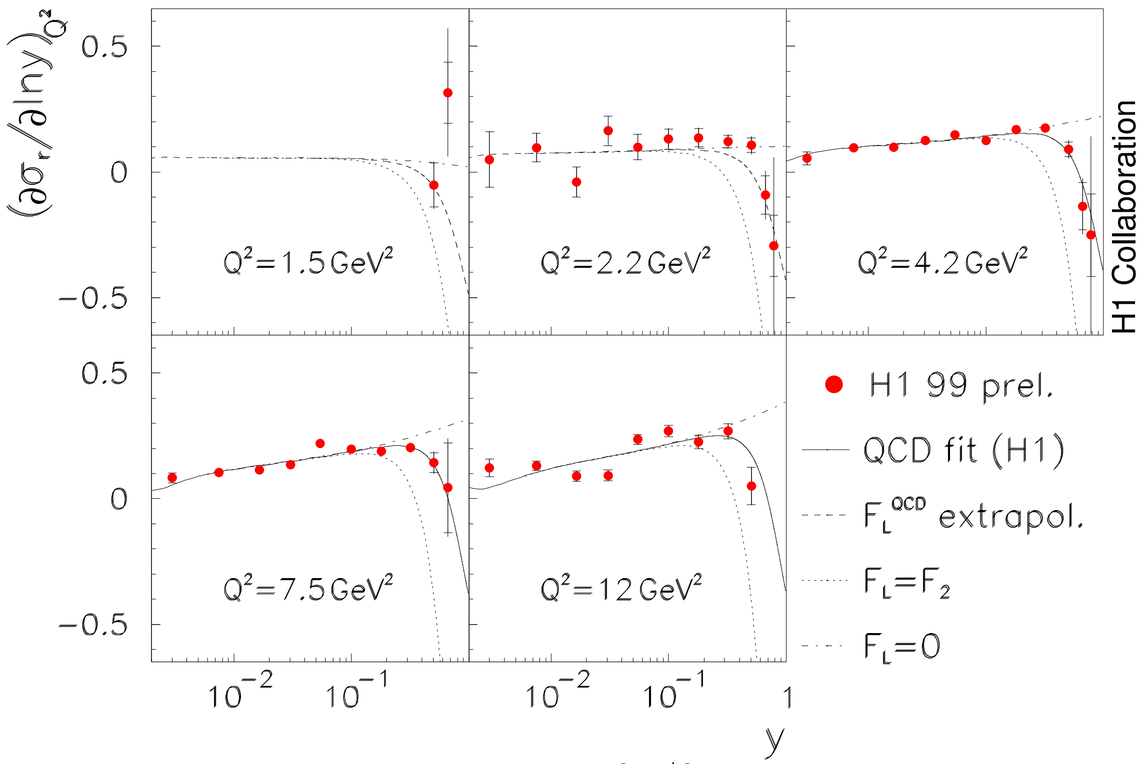

Figure 5: The reduced cross section derivative, $\partial\sigma_r/\partial \ln y$ as measured by the H1 Collaboration. The measurements are show as a function of y for different values of Q^2. Once again, the effect of $F_L(x, Q^2)$ at high y is visible.

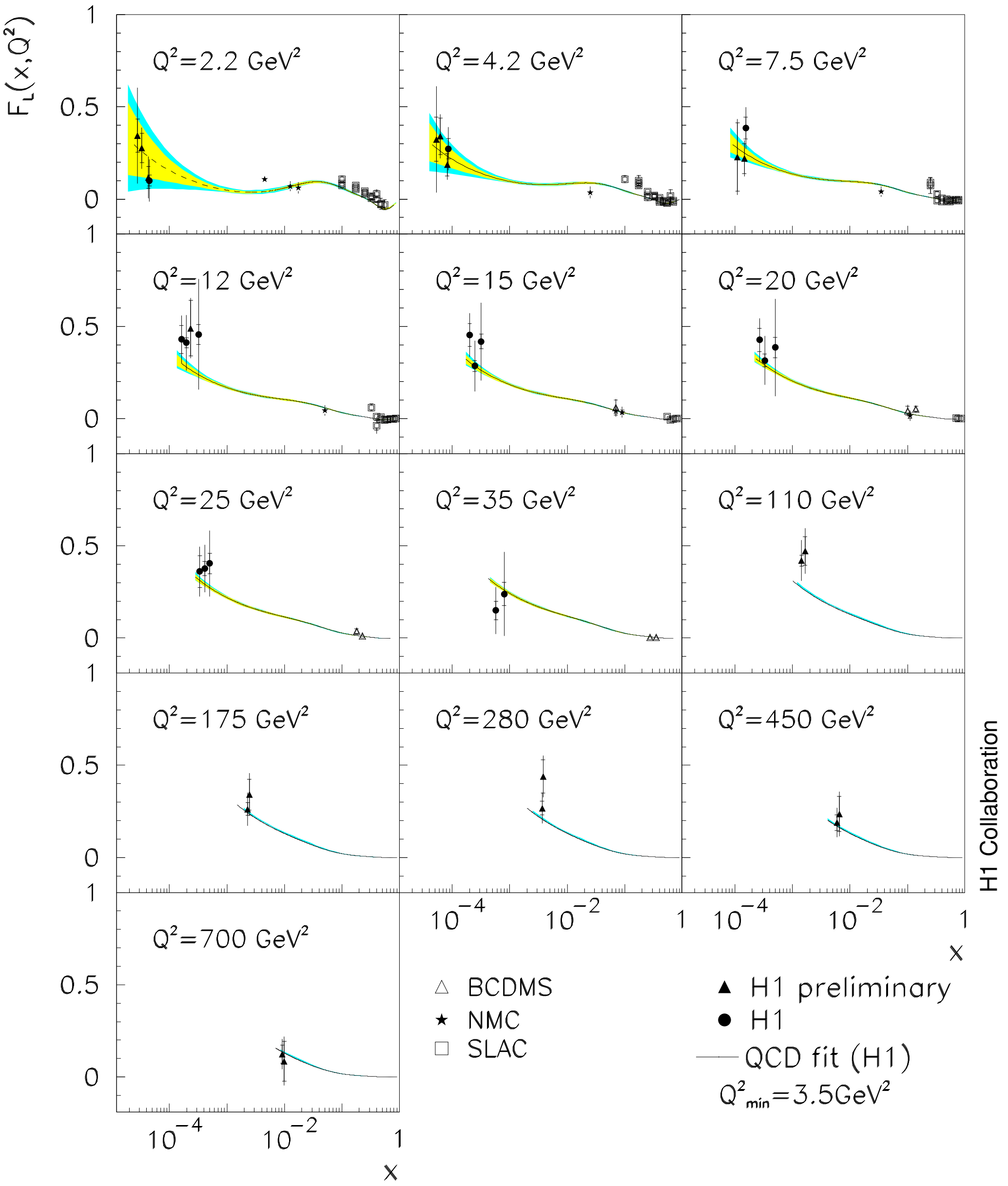

Figure 6: The longitudinal structure function, $F_L(x, Q^2)$ extraction from H1 data and from the fixed target experiments. The points are shown as a function of x for different values of Q^2. The dots are extracted using the first method described in the text, while the solid triangles are extracted using the second method. The data are compared to the predictions of the NLO QCD fit made by the H1 Collaboration.

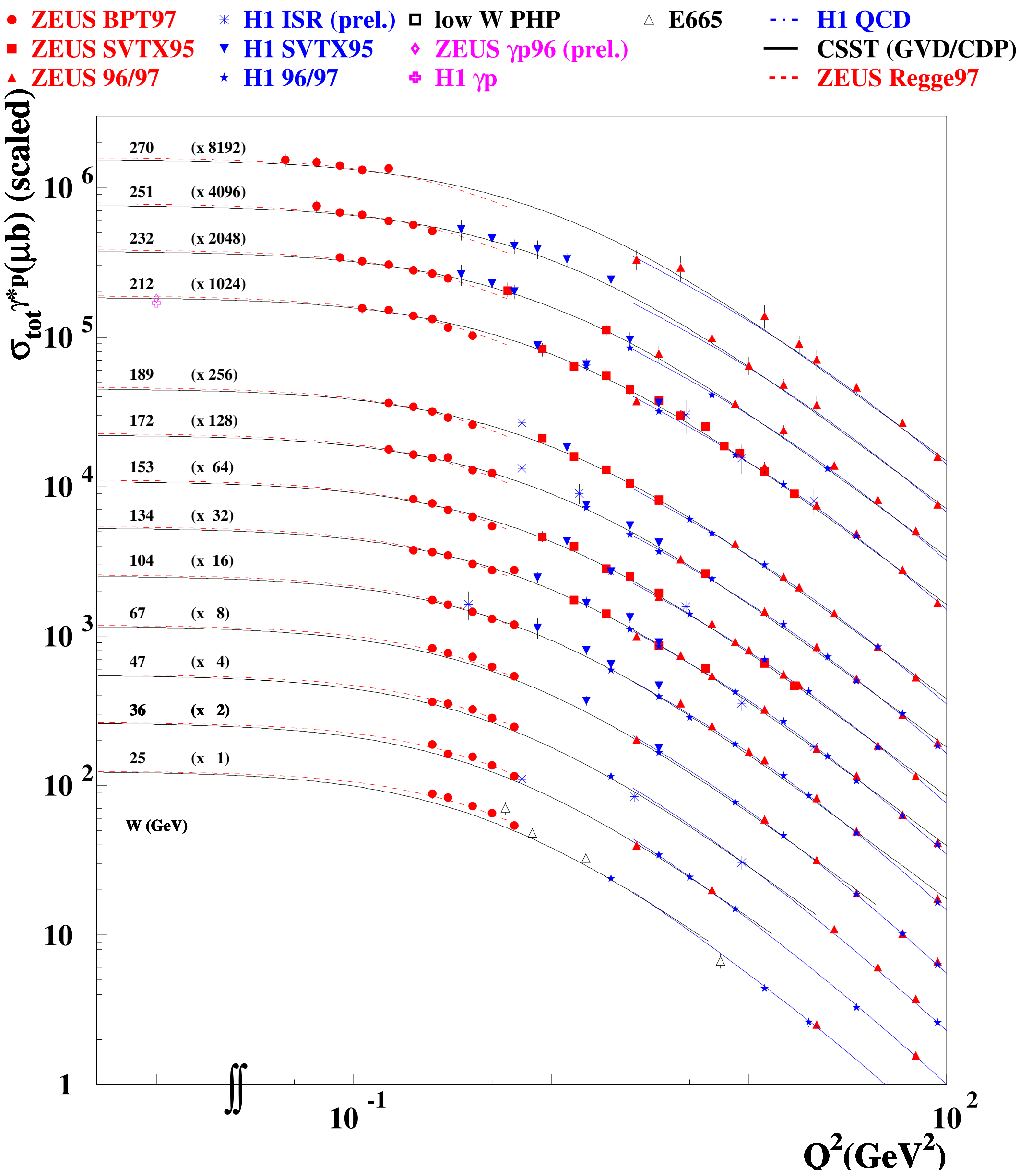

Figure 7: The total cross section $\sigma_{TOT}^{\gamma^* p}$ as a function of Q^2 for different values of W. The results from both HERA and the fixed target experiments are shown and are compared to the same theoretical predictions as used for comparison to the $F_2(x, Q^2)$ measurements shown earlier.

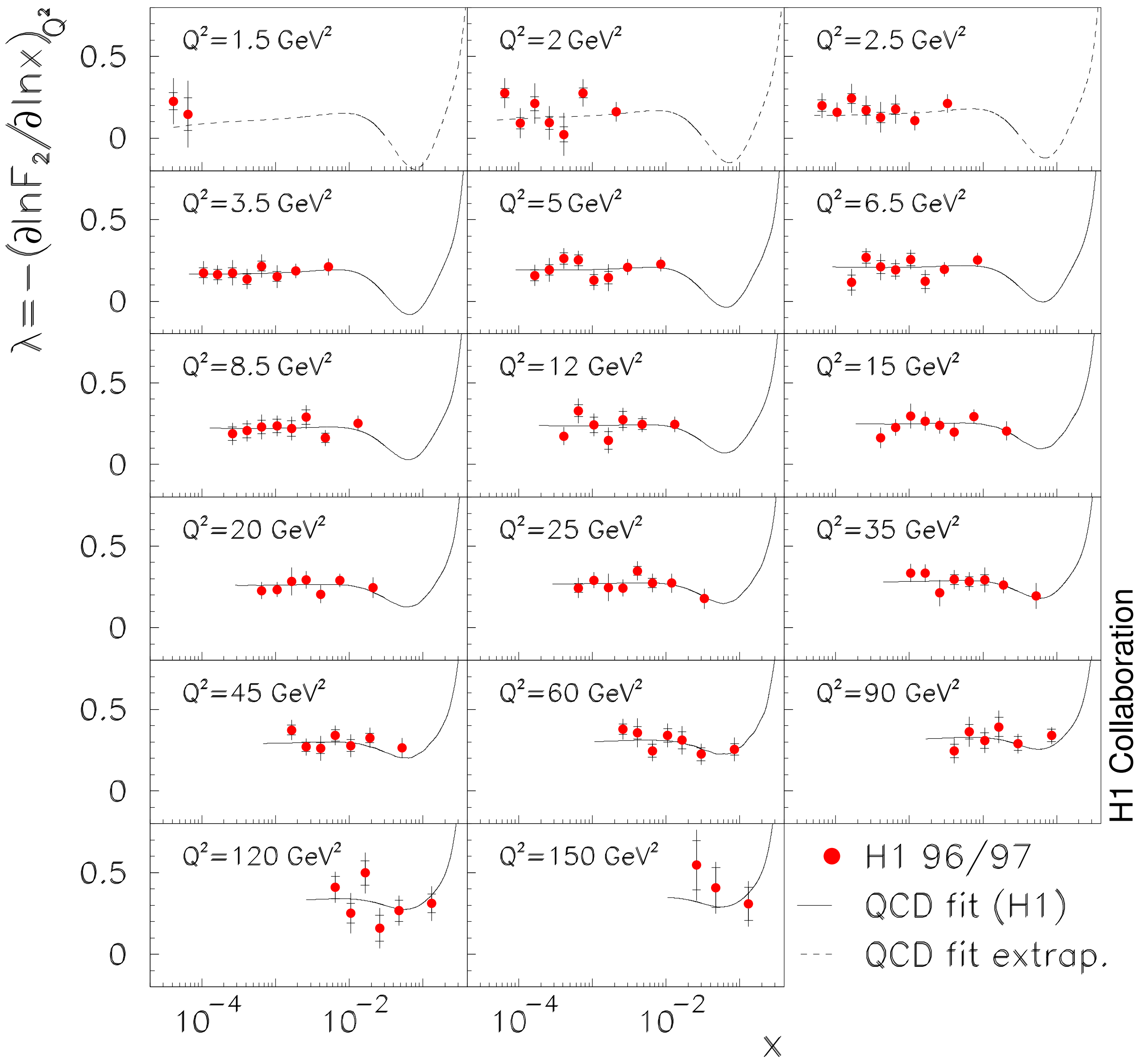

Figure 8: The partial derivative of $F_2(x, Q^2)$ with respect to $\ln x$ (also referred to as λ) as determined by the H1 Collaboration. The results are shown as a function of x for different values of Q^2. The solid lines are the predictions of the NLO QCD fit made by the H1 Collaboration. The dotted lines show the extrapolation of this fit to lower Q^2 values.

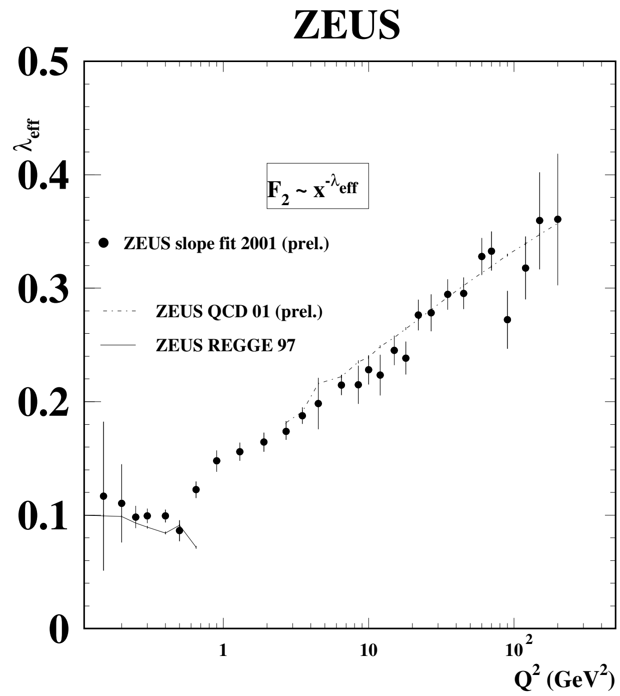

Figure 9: The variation of λ with Q^2, as determined by the ZEUS Collaboration. The results are compared to the predictions from the NLO QCD and Regge-based fits made by the ZEUS Collaboration. There is a clear change in the dependence of λ on Q^2 in the region around $Q^2 = 1$ GeV^2.

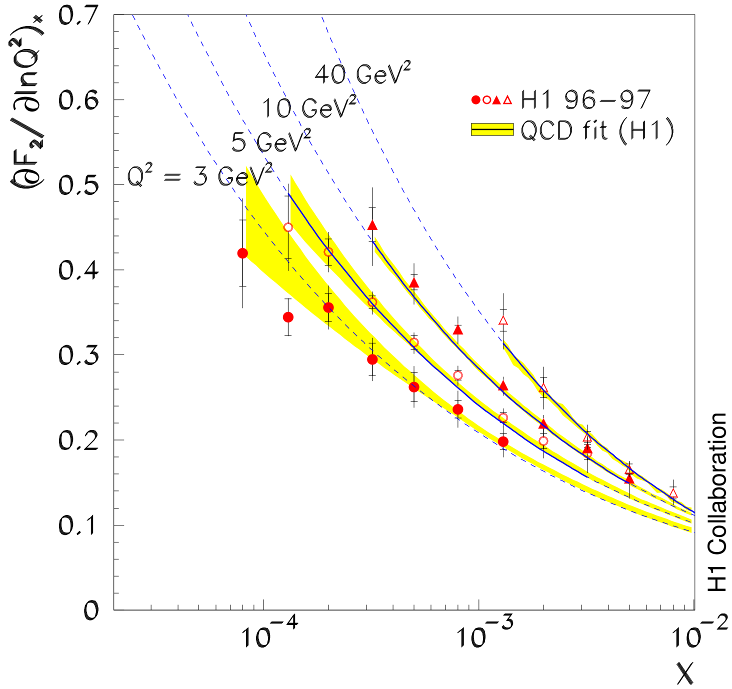

Figure 10: The partial deriative of $F_2(x, Q^2)$ with respect to $\ln Q^2$, as determined by the H1 Collaboration. The results are shown as a function of x for different values of Q^2. A comparison is made with the predictions of the NLO QCD fit made by the H1 Collaboration. The data and theory are consistent.

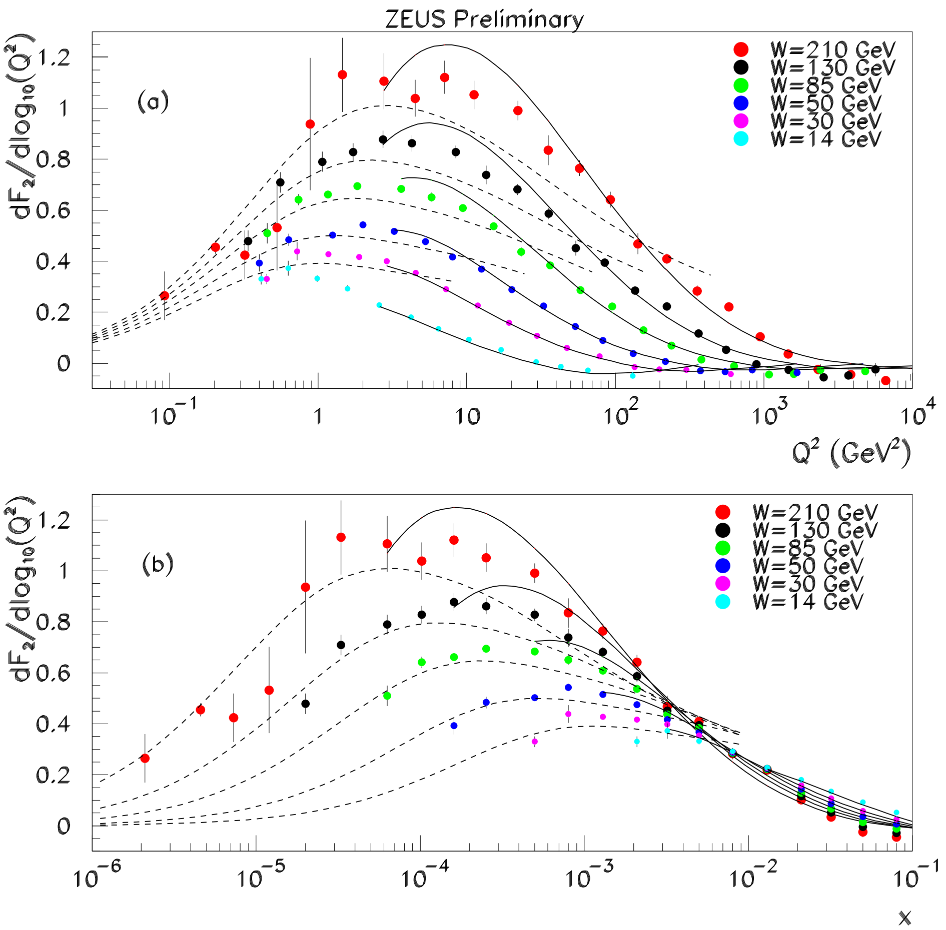

Figure 11: The partial derivative $\partial F_2/\partial \log Q^2$, this time determined by the ZEUS Collaboration. Here the data are shown as a function of x and Q^2 for different values of W. The solid lines are the predictions of the NLO QCD fit made by the ZEUS Collaboration, while the dotted lines are predictions from the model of Golec-Biernat and Wüsthoff, more details of which are given in the text. Both predictions give a reasonable description of the data.

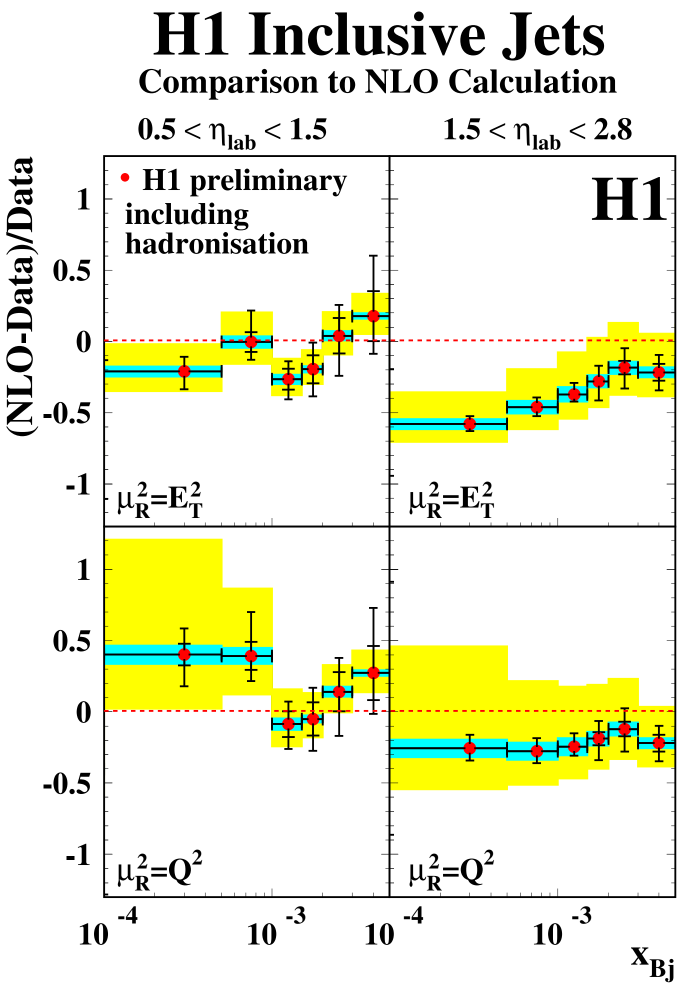

Figure 12: A comparison of inclusive jet measurements made by the H1 Collaboration with the predictions of NLO QCD. The results are shown as a function of x in two bins of pseudorapidity. The predictions are made assuming different values for the renormalisation scale and comparisons are made to both. There is a significant discrepancy between the data and theory at low x and high η_{jet} if the renormalisation scale is set to E_T^2. The origins of this discrepancy are not clear.